Optics Letters

Micro-transfer-printed short-wave infrared InP-on-silicon tunable laser

Xin Guo,[1,2,*] Emadreza Soltanian,[1,2] Jing Zhang,[1,2] Senbiao Qin,[1,2] Nicolas Vaissière,[3] Delphine Néel,[3] Joan Ramirez,[3] Jean Decobert,[3] Sarah Uvin,[1,2] and Gunther Roelkens[1,2]

[1]Photonics Research Group, Department of Information Technology, Ghent University-imec, 9052, Ghent, Belgium
[2]Center for Nano- and Biophotonics, Ghent University, 9052, Ghent, Belgium
[3]III-V Lab, Avenue Augustin Fresnel 1 F91767 Palaiseau, France
*Xin.Guo@UGent.be

Received 21 November 2024; revised 3 February 2025; accepted 10 February 2025; posted 11 February 2025; published 24 February 2025

We report an indium phosphide (InP)-on-silicon laser operating at short-wave infrared (SWIR) wavelengths, realized using micro-transfer printing (μTP) technology. Through thermal tuning of the integrated micro-ring resonators, the device is tunable from 1643 nm to 1707 nm, with mW-level output power at room temperature for a drive current of 100 mA on an amplifier. The laser cavities are fabricated on 200 mm silicon-on-insulator (SOI) wafers, featuring a 220 nm thick silicon device layer.

https://doi.org/10.1364/OL.549540

Introduction. Heterogeneous integration of III–V materials on silicon photonic integrated circuits (PICs) has emerged as a transformative approach to realizing on-chip laser sources. Indium phosphide (InP) and gallium arsenide (GaAs) are the primary III–V material systems employed for telecommunications wavelengths, particularly the O-band (1.3 μm) and the C-band (1.55 μm) [1]. Beyond these traditional bands, silicon photonics has significant potential for other applications, particularly in the short-wave infrared (SWIR) range, where integrated photonics can enable advanced solutions in sensing, spectroscopy, and environmental monitoring [2].

In the last decade, various methods have been developed to demonstrate O-band and C-band tunable lasers [3–6]. However, expanding tunable laser capabilities beyond the classical telecom band remains an underexplored yet valuable area. Such laser can be the key component to an on-chip spectroscopy sensing system for gases, where molecules such as methane and carbon dioxide exhibit prominent absorption features [7]. Despite these opportunities, integrating III–V materials such as InP onto silicon poses challenges, primarily due to material property mismatches and the need for efficient coupling between the III–V and silicon photonic components [8]. Recently, a hybrid integration approach has been reported using silicon nitride based PICs with a tunable range of 1634–1777 nm, relying on an external gain chip [9]. While this method provides a broad tuning range, it requires hybrid integration techniques and external gain components, which may limit the scalability and compactness of the solution.

Micro-transfer printing (μTP), a technology under license from X-Celeprint, has emerged as a promising solution to these integration hurdles, facilitating the precise placement of pre-fabricated, pre-tested III–V devices onto silicon substrates with high yield and minimal material waste [10,11]. This technique employs an elastomeric polydimethylsiloxane (PDMS) stamp to transfer III–V structures from their native wafers to silicon platforms, enabling wafer-scale integration with minimal disruption to the established silicon photonic manufacturing processes. μTP supports the efficient assembly of complex photonic systems by marrying the high performance of III–V materials with the scalability of silicon photonic technology.

In this work, we introduce a widely tunable InP laser covering 1643–1707 nm, integrated onto a silicon platform using μTP technology. The laser shows a maximal power of 2 mW in the waveguide. Our approach leverages the use of InP-based semiconductor optical amplifiers (SOAs) as the gain medium within the laser cavity, fabricated on 200 mm silicon-on-insulator (SOI) wafers together with micro-heaters for laser tuning.

Design and simulation. The laser cavity consists of silicon photonic circuits and the InP SOA; the latter one is transfer-printed onto the circuit during the post-process. By modifying the composition of the epitaxial layer stack, we can shift the gain spectrum to longer wavelengths [12]. Table 1 shows the epitaxial layer structure for this work, featuring a photoluminescence (PL) peak centered at 1650 nm.

The schematic of the whole circuit is shown in Fig. 1. The length of the SOA is 1 mm, with a pair of adiabatic tapers at each side to realize an efficient coupling between the SOA and the underlying Si waveguide [13]. A Mach–Zehnder interferometer (MZI) consisting of two MMIs is used as a tunable outcoupling mirror. Besides, a thermo-optic phase tuning section is employed to adjust the position of the cavity modes. The wavelength selection is achieved through a pair of thermally tunable micro-ring resonators (MRRs) with slightly different radii of 32 μm and 30 μm. These MRRs form a Vernier filter, which provides an expanded effective free spectral range (FSR) compared

Table 1. SOA Epitaxial Layer Stack

Layer Type	Material	Thickness (nm)
P-contact	InGaAs	200
P-doped	InP	1500
SCH	AlGaInAs	50
Barrier × 6	AlGaInAs	10
Well × 6	AlGaInAs	6
Barrier	AlGaInAs	10
SCH	AlGaInAs	50
N-doped	InP	200
Sacrificial 1	InGaAs	50
Sacrificial 2	AlInAs	500

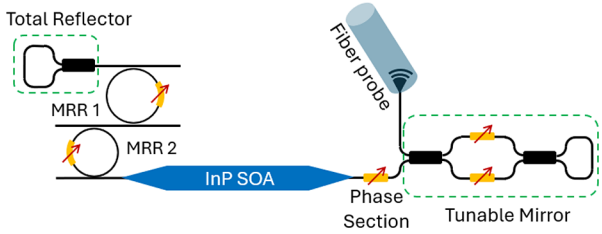

Fig. 1. Schematic of an InP tunable laser.

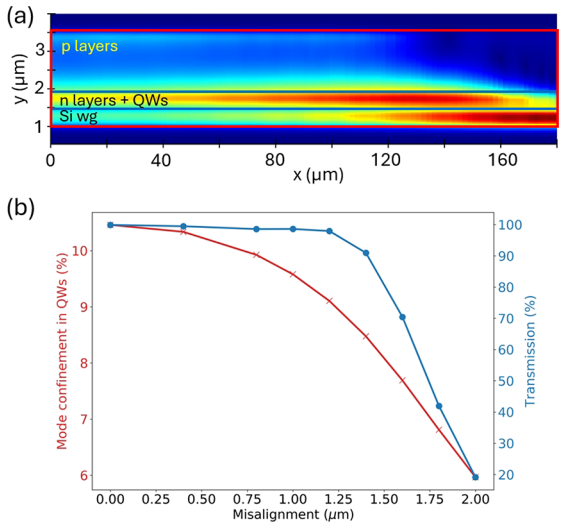

Fig. 2. Simulation of light coupling from the III–V to silicon waveguides. (a) Simulated intensity distribution showing the coupling between the Si waveguide and the III–V layers. (b) Relationship between mode confinement and transmission efficiency as a function of μTP misalignment between the silicon waveguide and III–V coupon.

to the individual resonators, resulting in a wider tuning range. Each ring resonator has an FSR of approximately 4 nm, while the combined FSR of the Vernier filter extends to around 62 nm within the targeted wavelength range. Figure 2 illustrates the optical coupling process and its impact on transmission and mode confinement. The III–V taper section narrows from 4 μm to 400 nm over a length of 180 μm, while the silicon waveguide remains 3 μm wide beneath the taper. Panel (a) shows the simulated intensity distribution for the coupling between the silicon waveguide and the III–V layers, demonstrating how the optical mode is gradually compressed into the silicon layers. Panel (b) depicts the dependence of mode confinement and transmission on the lateral misalignment between the silicon and III–V waveguides. With the current μTP tool, an alignment accuracy of ±0.5 μm at 3σ can be achieved, ensuring adiabatic coupling.

The epitaxial layer structure was grown by metal-organic vapor-phase epitaxy (MOVPE). The fabrication of the SOA device coupons on the source wafer consists of a series of electron beam and optical lithography steps, combined with wet and dry etching processes and metal contact deposition, similar to the process discussed in [3].

After the mesa has been patterned (Fig. 3(a)), the n-contact is deposited, followed by n-InP etching, and etching of the GaInAs and AlInAs release layers, together with a few hundred nanometers into the InP substrate. Next, a SiNx layer was deposited and patterned to form tethers that will keep the devices in place during the selective chemical etching of the release layer (Fig. 3(b)). The whole device was then encapsulated by a thick layer of DVS-BCB, which was thinned down until the top of the p-mesa. The DVS-BCB is patterned to expose the patterned SiN tether structures around the coupon mesa. Then, the p-metal is deposited, followed by n-via opening to expose the n-metal and DVS-BCB removal in the tether area. To provide extra support for the coupon during the release etching (Fig. 3(d)) using a FeCl3 wet-etch, a layer of Ti35E photoresist is spin-coated and defined within the coupon regions on the chip.

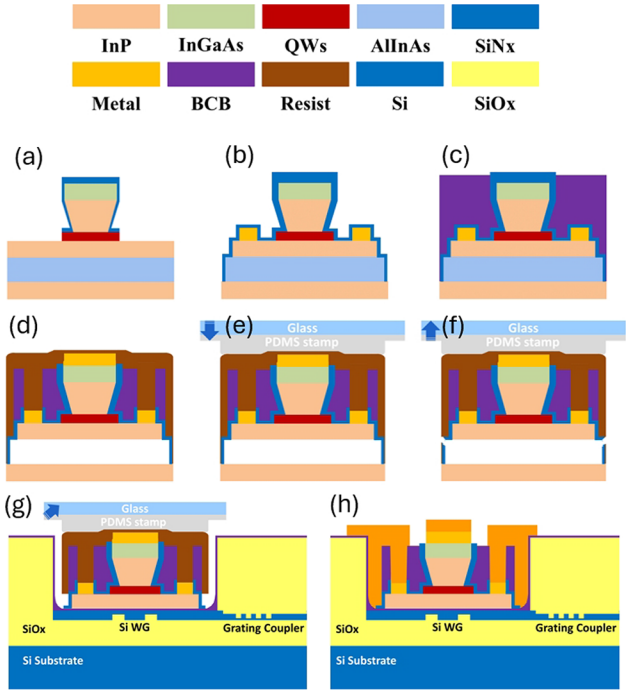

Fig. 3. Schematic of the process flow: (a) InP SOA mesa patterning, (b) n-metal deposition and μTP layer etching and SiNx passivation, (c) BCB planarization, (d) p-metal deposition and encapsulation, and (e)–(h) μTP process and final metallization.

The μTP process is facilitated by an X-Celeprint μTP-100 tool. A dedicated PDMS stamp, dimensioned to match the coupon, is employed to transfer the coupons onto the target photonic integrated circuit (PIC) chip. The PDMS stamp lifts the coupon from the source wafer by breaking the tethers and subsequently transfers it by laminating the stamp onto the target wafer. After the lamination, the stamp is released for the

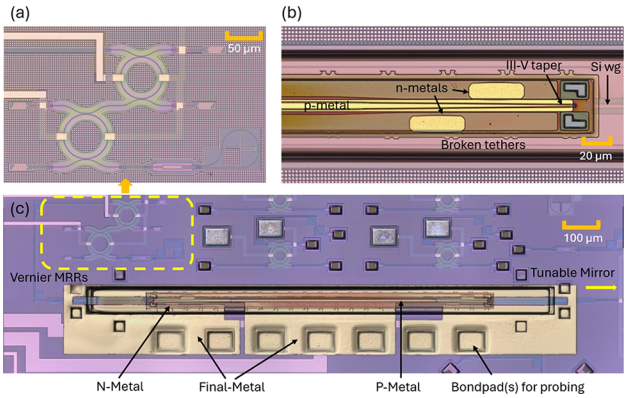

Fig. 4. Microscope image of a fabricated laser. (a) Vernier filter. (b) Transfer-printed InP coupon into the trench of the target chip. (c) Transfer-printed InP tunable laser on SOI after final metalization.

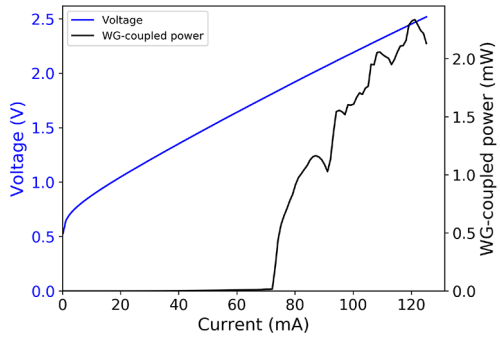

Fig. 5. L–I–V curve of the laser with a lasing wavelength at 1665 nm.

next printing cycle (Fig. 3(e)). To achieve high printing yield, a DVS-BCB layer (1:5 solution) is spray-coated onto the target sample, followed by a soft bake at 150°C for 10 min to reflow the DVS-BCB, ensuring a smooth printing process. This bonding material ultimately forms a 10–30 nm layer between the III–V coupon and the silicon waveguide. The initial experiments demonstrate a printing yield of 98%, indicating the robustness of the process. Finally, the protective photoresist is removed by an oxygen-plasma etch, and additional metallization (Fig. 3(h)) is applied to facilitate wire-bonding or probing on the target wafer. Figure 4 shows the microscope image of a fabricated laser.

Characterization. The L–I–V characteristics of the InP tunable laser were measured to assess its performance at 1665 nm. The measurements were performed on a temperature-controlled stage maintained at 20°C to ensure thermal stability. The laser is controlled by Keithley 2400 Sourcemeters, and the output of the laser is coupled to a single-mode fiber (SMF), which is connected to a HP 81532A power sensor. Figure 5 shows that the laser has a threshold current of approximately 75 mA and reaches a maximum output power of about 2.2 mW at 120 mA. The output power shows irregular, step-like fluctuations beyond the threshold current, which are indicative of mode hopping. The I–V curve indicates a differential resistance of 13 Ω at the maximum current of 120 mA.

The full spectral tuning of the demonstrated tunable laser was measured under a constant injection current of 100 mA and is shown in Fig. 6(a). The coupling loss of each grating coupler is around 7.5 dB. The laser exhibits a broad tuning range from

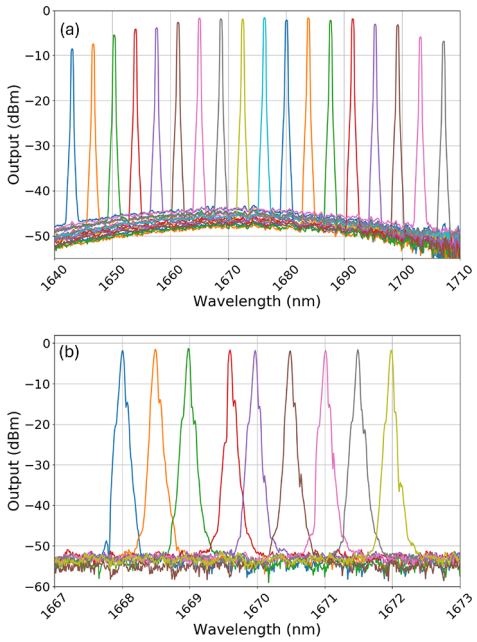

Fig. 6. Wavelength tuning results at 20°C: (a) full tuning spectrum and (b) fine-tuning from 1668 nm to 1672 nm.

1643 nm to 1707 nm, covering a total range of 64 nm. The tuning was achieved through thermo-optic phase tuning of one of the MRRs. The peaks are evenly spaced by approximately 4 nm, with the combined free spectral range (FSR) of the Vernier filter measured to be approximately 60 nm, aligning with the expected design.

In addition to the coarse spectral tuning, fine-tuning of the demonstrated laser was achieved by thermally tuning both the MRRs and phase section, as shown in Fig. 6(b). This approach enabled fine wavelength adjustments in steps of 0.5 nm, covering a tuning range from, e.g., 1668 nm to 1672 nm (requiring about 16 mW additional power dissipation in both ring heaters), matching with the 4 nm spacing from Fig. 6(a), indicating that all wavelengths over the >60 nm tuning range are accessible. The spectrum exhibits narrow main peaks corresponding to the lasing wavelength, with minor side features attributed to artifacts introduced by the optical spectrum analyzer (OSA).

Besides, we investigated the thermal tuning behavior of the MRRs. Figure 7 shows the lasing wavelength as the laser is coarsely (1647–1666 nm) tuned using the heater on MRR 1. As the heater power increases, the laser wavelength increases linearly. A linear fit (red dashed line) indicates a tuning efficiency of 5 nm/10 mW.

To contextualize our results, we compared the performance of our InP tunable laser with similar devices reported in the literature. Our laser demonstrates a peak output power of 2.2 mW, while a previously reported micro-transfer-printed (μTP) tunable laser at 1580 nm achieved 1 mW [14]. Additionally, a classical μTP laser at the C-band [4] achieved a 5 dB increase in peak power but exhibited less stable output power across the tuning range. Regarding the tuning range, our laser achieves an FSR of 64 nm, compared to the 40 nm FSR of the previously mentioned 1580 nm laser and the 54 nm FSR of the C-band laser. This preliminary demonstration highlights the effectiveness of our design, with room for improvement through parameter optimization. The extension to longer wavelengths faces increased

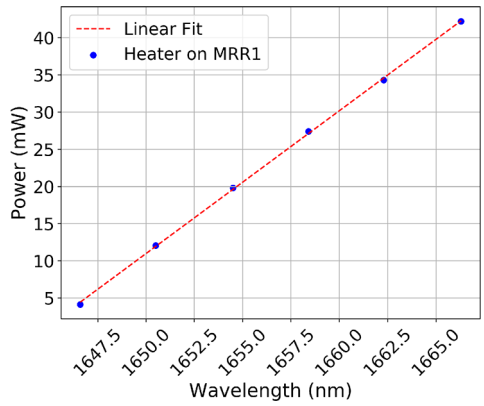

Fig. 7. Dependence of the lasing wavelength on the electrical power dissipated in MRR 1.

Auger recombination losses in the epitaxial layers, underscoring the critical role of active region optimization for an efficient performance.

Conclusion. This paper reports the design, fabrication, and characterization of a widely tunable short-wave infrared InP-based laser integrated onto a silicon photonic platform via μTP. The laser operates across the 1643–1707 nm range, achieving a broad tuning range through a Vernier filter with a combined FSR of over 60 nm. Fine-tuning capabilities are demonstrated, and the output power reaches 2.2 mW. The results underscore the potential of μTP for integrating III–V materials with silicon photonics, enabling tunable lasers for applications in the short-wave infrared (SWIR) range, including spectroscopy and environmental sensing.

Acknowledgment. The authors would like to thank Dr. Biwei Pan and Dr. Yang Liu for their valuable discussion on III–V laser integration.

Disclosures. The authors declare no conflicts of interest.

Data Availability. Data underlying the results presented in this paper are not publicly available at this time but may be obtained from the authors upon reasonable request.

REFERENCES

1. C. Xiang, W. Jin, D. Huang, *et al.*, IEEE J. Sel. Top. Quantum Electron. **28**, 1 (2022).
2. L. Rothman, I. Gordon, Y. Babikov, *et al.*, J. Quant. Spectrosc. Radiat. Transfer **130**, 4 (2013).
3. A. Malik, J. Guo, M. A. Tran, *et al.*, Photonics Res. **8**, 1551 (2020).
4. E. Soltanian, G. Muliuk, S. Uvin, *et al.*, Opt. Express **30**, 39329 (2022).
5. M. A. Tran, D. Huang, J. Guo, *et al.*, IEEE J. Sel. Top. Quantum Electron. **26**, 1 (2020).
6. J. Zhang, L. Bogaert, C. Krückel, *et al.*, Opt. Express **31**, 42807 (2023).
7. T. Gruendl, K. Zogal, M. Mueller, *et al.*, *Optics in Atmospheric Propagation and Adaptive Systems XIII*, Vol. 7828 K. Stein and J. D. Gonglewski, eds., International Society for Optics and Photonics (SPIE, 2010), p. 782807.
8. G. Roelkens, A. Abassi, P. Cardile, *et al.*, Photonics **2**, 969 (2015).
9. F. Farjana, A. van Rees, and D. Geskus, *The 25th European Conference on Integrated Optics*, J. Witzens, J. Poon, L. Zimmermann, and W. Freude, eds. (Springer Nature, 2024), pp. 3–7.
10. G. Roelkens, J. Zhang, L. Bogaert, *et al.*, APL Photonics **9**, 010901 (2024).
11. J. Zhang, G. Muliuk, J. Juvert, *et al.*, APL Photonics **4**, 110803 (2019).
12. R. Wang, A. Vasiliev, M. Muneeb, *et al.*, Sensors **17**, 1788 (2017).
13. B. Haq, S. Kumari, K. Van Gasse, *et al.*, Laser Photonics Rev. **14**, 1900364 (2020).
14. J. Zhang, Y. Li, S. Dhoore, *et al.*, Opt. Express **25**, 7092 (2017).